ACS Catalysis

Research Article

Cite This: ACS Catal. 2018, 8, 9056−9065

pubs.acs.org/acscatalysis

Cooperative Catalysis by Surface Lewis Acid/Silanol for Selective Fructose Etherification on Sn-SPP Zeolite

Tyler R. Josephson,*[,†,‡,§] Robert F. DeJaco,[§] Swagata Pahari,[‡] Limin Ren,[§] Qiang Guo,[§] Michael Tsapatsis,[§] J. Ilja Siepmann,[‡,§] Dionisios G. Vlachos,[†] and Stavros Caratzoulas[†]

[†]Department of Chemical and Biomolecular Engineering, Harker Interdisciplinary Science and Engineering Laboratory, University of Delaware, 221 Academy Street, Newark, Delaware 19716, United States

[‡]Department of Chemistry, University of Minnesota, 139 Smith Hall, 207 Pleasant Street SE, Minneapolis, Minnesota 55455, United States

[§]Department of Chemical Engineering and Materials Science, University of Minnesota, 151 Amundson Hall, 412 Washington Avenue SE, Minneapolis, Minnesota 55455, United States

Supporting Information

ABSTRACT: While Lewis-acid zeolites, such as Sn-Beta, catalyze glucose isomerization in an alcoholic medium, mesoporous Sn-SPP catalyzes both glucose isomerization to fructose and fructose etherification (formally ketalization) to ethyl fructoside, enabling fructose yields in excess of the glucose/fructose equilibrium. Using periodic density functional theory calculations and force-field-based Monte Carlo simulations, the ketalization reaction mechanism and adsorption behavior were examined. The silanols on the Sn-SPP mesopore surface facilitate the ketalization reaction through hydrogen bonding interactions at the transition state, only possible via a Sn−O−Si−OH moiety, present in Sn-SPP but not in Sn-Beta. Fructose ketalization is favored over glucose acetalization due to differences in stability of the oxonium intermediates, which are stabilized by the Sn-SPP active site. The open site of hydrophobic Sn-Beta cannot perform these reactions because its active site does not contain an adjacent silanol of the right geometry. In addition to the more favorable activation barrier of the catalytic process, the adsorption at the catalytic site in Sn-SPP is also found to be more favorable than for Sn-Beta, in spite of competitive adsorption between fructose and ethanol in the ethanol-saturated zeolites.

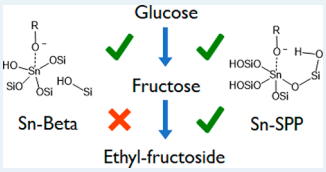

KEYWORDS: *biomass processing, sugars chemistry, ketalization, acetalization, Gibbs ensemble Monte Carlo, adsorption*

1. INTRODUCTION

In the integrated "biorefinery" concept, cellulose, hemicellulose, and lignin fractions of biomass are separated, processed, and upgraded into a diverse slate of chemical products, akin to crude oil processing in a refinery.[1−5] In particular, furan derivatives such as 5-hydroxymethylfurfural are promising platform chemicals derived from sugars.[6−8] While aldoses such as glucose and xylose are abundant as major constituents of cellulose and hemicellulose, ketoses are more valuable for their higher yields to furans.[9] Therefore, ketose/aldose isomerization is a key reaction for enabling the furans platform for renewable chemicals.

Lewis acidic zeolites such as Sn-Beta have been demonstrated to convert glucose[10] and xylose[11] into fructose and xylulose, respectively, via an intramolecular 1,2-H-shift reaction.[12] These catalysts have achieved 33% yield[10] to fructose in aqueous media, with a 9% yield to mannose, approaching the ∼50% equilibrium yield achieved with the glucose isomerase enzyme.[13] One strategy for boosting the fructose yield beyond the glucose/fructose equilibrium was proposed by Saravanamurugan and co-workers[14] (see Scheme 1). When glucose was reacted in methanolic solutions with H-USY zeolite, the fructose product formed an ether with methanol, producing methyl fructoside and shifting equilibrium toward the products. Subsequent addition of water restored the fructoside to fructose, producing a total fructose yield of over 55%.[14] In ethanol, however, H-USY catalyzed the acetalization of glucose as well, reducing yields to the fructose product, although side reactions can be reduced by optimizing the ratio of Lewis and Brønsted acids in the zeolite.[15] The same authors have also found H-USY to be useful for acetalization of furfural.[16]

Ren and co-workers have also demonstrated glucose isomerization/fructose ketalization over the hierarchical tin-containing zeolite. Using the self-pillared pentasil Sn-SPP zeolite, consisting of MFI sheets with 0.5 nm pores and containing larger mesopores (see Figure 1), a fructose yield of 65% was achieved using a similar reaction procedure in ethanol.[17] The hierarchical mesoporous structure of Sn-SPP also permitted isomerization of disaccharides. Pillared Sn-MWW, based on another zeolite framework, has also been shown to be active for mono- and disaccharide isomerization through the same tandem reaction procedure.[18] A remarkable feature of both catalysts is the suppression of the glucose acetal

Received: April 25, 2018
Revised: August 14, 2018
Published: August 20, 2018

DOI: 10.1021/acscatal.8b01615
ACS Catal. 2018, 8, 9056−9065

Scheme 1. Reaction Scheme for Improving Fructose Yields from Glucose Using Tandem Reactions with Fructose Ketalization

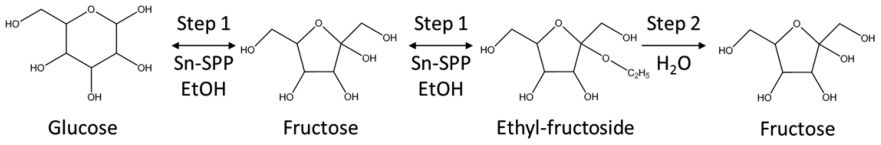

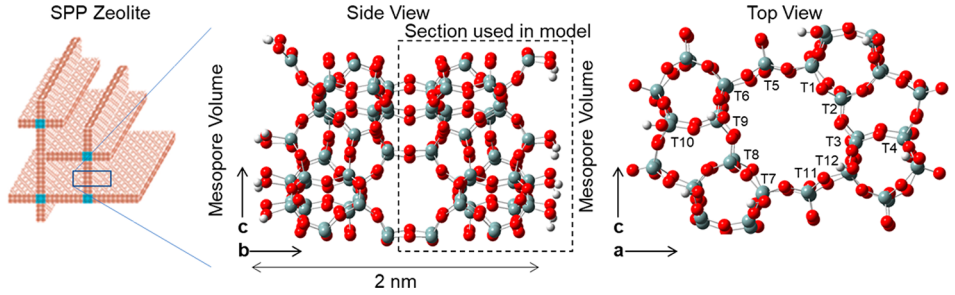

Figure 1. Structure of the self-pillared pentasil (SPP) zeolite. The cage walls are comprised of intergrown 2D layers of MFI framework zeolite, with a 2 nm thickness corresponding to the width of the *b* axis of the MFI unit cell. The catalyst model was constructed using one-half of the MFI unit cell (dashed box), each side of which is terminated by eight silanol groups per unit cell.

product. Interestingly, another mesoporous, Sn-containing zeolite, three dimensionally ordered mesoporous imprinted (3DOm-i) Sn-MFI was found to be active for glucose isomerization, but not fructose ketalization, in methanol.[19]

The reaction of fructose to ethyl fructoside is formally a ketalization reaction. Acetals and ketals are textbook protecting groups and are effective for stabilizing aldehydes and ketones and protecting them from attack by nucleophiles and bases.[20] While Brønsted acid catalysis mechanisms have been proposed using organic chemistry principles,[20] we have not found any proposed mechanisms for Lewis acid catalysis, and no theoretical study has examined either Brønsted or Lewis acid-catalyzed (ace)ketalization mechanisms. Moreover, the experimental data do not provide insight into how these pillared, Lewis-acidic zeolites catalyze the fructose ketalization but not the glucose acetalization, nor why other Lewis acid catalysts, such as Sn-Beta, catalyze the isomerization but not the ketalization, in alcoholic media.

In this work, we apply electronic structure calculations to characterize the active site in Sn-SPP and show the importance of the Sn−O−Si-OH moiety for the catalysis of the ketalization, which is present in Sn-SPP but not in Sn-Beta. Monte Carlo simulations complement the electronic structure calculations by providing information on the competitive adsorption of fructose and ethanol from solution onto the catalytic porous materials and also show that fructose adsorbs onto the Sn-SPP more favorably than in Sn-Beta.

2. METHODS

Periodic density functional theory (DFT) calculations were performed using the GPAW software[21,22] in the ASE framework.[23] Core electrons were represented with the PAW formalism,[24,25] while the valence electrons were represented with the Perdew−Burke−Ernzerhof (PBE) exchange-correlation functional.[26] Optimizations using PBE were performed using the quasi-Newton limited memory Broyden−Fletcher−Goldfarb−Shanno (LBFGS) optimizer.[27] Reaction pathways were computed using the nudged elastic band (NEB) method[28] with typically 8−12 images between local minima, with transition states identified using the dimer method.[29−32] Initial optimizations used a double-ζ plus polarization (DZP) linear combination of atomic orbitals (LCAO) basis set,[33] with final optimizations performed using the finite difference approach with a grid spacing of 0.2 Å. Electronic energies were optimized to a precision to 10^{-6} eV and atomic coordinates were optimized to a force convergence threshold of 0.05 eV $Å^{-1}$. Dispersion corrections for reactants, products, intermediates, and transition states were estimated using Grimme's DFT-D3 method,[34] and results with and without dispersion are compared in Table S1−S5. Frequencies and free energy corrections were calculated using finite differences, with a grid spacing of 0.18 Å and a tighter SCF convergence (10^{-8} eV). All calculations were performed at the Γ-point.

Monte Carlo simulations in the isobaric—isothermal version of Gibbs ensemble were performed at T = 363 K and p = 1.7 bar, following similar procedures as in previous work.[35,36] The total number of molecules consisted of 15 fructose molecules, 8 impurity molecules with scaled nonbonded interaction parameters, and 700 or 1000 ethanol molecules for the systems with Sn-Beta or Sn-SPP, respectively. Additional details regarding the methodology of the molecular simulations are provided in the Supporting Information.

3. ACTIVE SITE OF SN-SPP

The self-pillared pentasil (SPP) zeolite is comprised of intergrown 2D layers of the MFI zeolite framework.[37] Transmission electron microscopy (TEM) has shown the wall thickness to be 2 nm (one unit cell) along the *b*-axis of MFI.[37] To model the SPP zeolite, we represent it as a single 2D layer of MFI zeolite, periodic in the *ac* plane, as shown in Figure 1. To accelerate the DFT calculations and focus on the surface chemistry, the zeolite was cut in half along the *b*-axis to yield a 1 nm-thick nanosheet, approximately halving the number of atoms in the calculation. The underside of the surface was terminated with hydrogens, and these were constrained, along with the layer of atoms within 7 Å of the bottom of the periodic cell (52 atoms).

MFI has 12 distinct crystallographic locations (see Figure 1). In the Sn-SPP zeolite, there are more, because some of these sites are present inside the interior of the zeolite layer while others are at the surface. However, because hexoses are not admitted into the micropores of MFI,[38] the relevant Sn site

DOI: 10.1021/acscatal.8b01615
ACS Catal. 2018, 8, 9056−9065

must be present at the surface. An inventory of these 12 surface sites on SPP is given in Table 1. Substituting Sn into each of these sites would generate a Sn site with different properties. Four sites are "terminal" sites, $HOSn(SiO)_3$ (T7, T9, T10, and T12), while the remaining eight sites are "closed" sites, $Sn(SiO)_4$. The "terminal" sites are located where the MFI framework is terminated at the surface and are distinct from the similar "open" sites of Sn-Beta, which are paired with a silanol produced through hydrolysis of a closed site or through incomplete condensation. The surface is densely populated with silanols; of the eight closed sites, two have three adjacent silanols (T8 and T11), four have one (T1, T3, T4, and T6), and two have zero (T2 and T5), although sites with zero adjacent SiOH have three or four next-nearest neighbor silanols (Table 1).

Table 1. Relative Stability of the Sn Substitution at 12 Surface Locations on the SPP Unit Cell, Calculated Using PBE-D3[a]

substitution	relative U (kcal/mol)	number of NN SiOH	type of site
T8	0	3	closed
T10	0.20	1	terminal
T9	0.72	1	terminal
T7	0.79	0	terminal
T12	1.96	0	terminal
T11	3.75	3	closed
T4	3.90	1	closed
T3	5.54	1	closed
T1	6.90	1	closed
T2	7.75	0	closed
T5	8.35	0	closed
T6	10.5	1	closed

[a]The local environment of each Sn is described in terms of the number of nearest-neighbor silanol groups (indicating Sn−O−Si−OH moieties) and whether or not the substitution occurs at a site where the MFI framework is terminated, generating a $HOSn(OSi)_3$, or a closed site, leading to $Sn(OSi)_4$. Note that the sites with 0 NN SiOH still have 3-4 next-nearest neighbor silanols. Relative stabilities calculated using PBE are reported in Table S5.

To identify the most energetically stable site for Sn substitution, we optimized the geometries of Sn-SPP with Sn in only one of these distinct sites. The T8 site is found to be energetically most stable, closely followed by the "open" sites T10, T9, T7, and T12. Because ^{119}Sn-NMR of Sn-SPP found evidence of only tetrahedrally coordinated "closed" Sn sites,[17] the T8 site was chosen as the site most consistent with the experimental and theoretical results. T8 has three adjacent silanols and is located at the boundary of the MFI pore (see Figure 1).

4. REACTION MECHANISM ANALYSIS

Ketalization occurs in two steps (Scheme 2a): addition of an alcohol to a ketone to form a hemiketal and reaction of another alcohol with the hemiketal, eliminating water and forming the ketal. For the ketalization of fructose, the O5 hydroxyl of fructose and the ethanol hydroxyl react with the C2 keto group, generating two overall paths for the formation of the ketal product (Scheme 2). Hemiketal formation with the O5 hydroxyl is synonymous with ring-closing and produces fructofuranose **2**, whose anomeric hydroxyl reacts with the ethanol, eliminating water and forming the ketal. Alternatively, the C2 keto group can first react with the ethanol hydroxyl to form hemiketal **3**, followed by ring-closing and water elimination with the O5 hydroxyl to form the ketal.

In the final ketalization steps, two hydroxyls react to form the ketal and a water molecule. Distinct pathways are possible depending on which hydroxyl oxygen is eliminated as water and which is retained in the ketal, producing ketals **4a**−**4d** (Scheme 2). Tracer experiments with ^{18}O-labeling on ethanol and O2/O5 of fructose could potentially discriminate among products **4a**, **4b**/**4c**, and **4d**, but no such data have been reported in the literature. Development of such techniques would be valuable for experimental validation of our proposed mechanism.

4.1. Hemiketal Formation Mechanisms. Lewis acid-catalyzed hemiketal formation has previously been studied in mechanistic studies of glucose isomerization that consider ring-opening and ring-closing reactions.[12,39−41] These involve either O2 (the ketone) or O5 (the alcohol) coordinating to the Sn site. Pathway A for hemiketalization begins with deprotonation

Scheme 2. Scheme Showing Hemiketalization Reactions of Open Fructose 1 to Fructofuranose 2 and Hemiketal 3, Followed by Two Pathways Each to Ketals 4a−d, Depending on Which Oxygen Is Eliminated in the Water Product

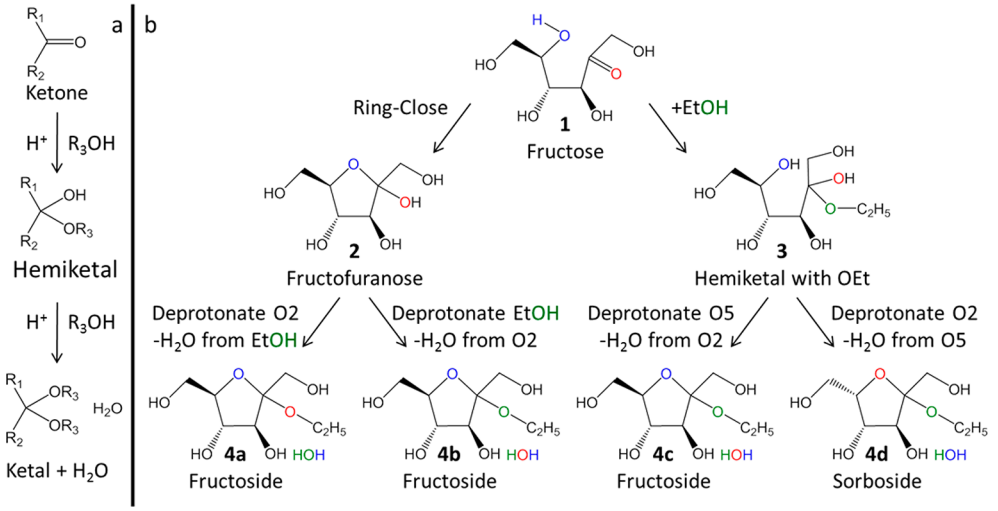

DOI: 10.1021/acscatal.8b01615
ACS Catal. 2018, 8, 9056−9065

Scheme 3. Summary of Ketalization Pathways[a]

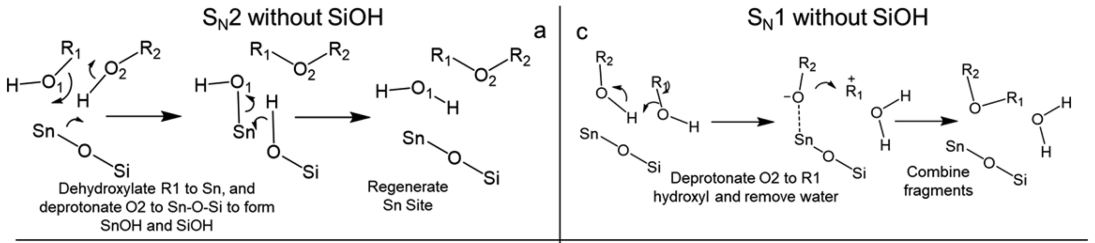

R1	R2	Product	Feasible?
Ethanol	C2	Ketal **4a**	Yes
C2	Ethanol	Ketal **4b**	No - Tertiary S_N2
C2	C5	Ketal **4c**	No - Tertiary S_N2
C5	C2	Ketal **4d**	No - Sorboside product

R1	R2	Product	Feasible?
Ethanol	C2	Ketal **4a**	No - Primary C^+
C2	Ethanol	Ketal **4b**	Yes
C2	C5	Ketal **4c**	Yes
C5	C2	Ketal **4d**	No - Sorboside product

[a](a) S_N2 pathway catalyzed by Lewis acid. (b) S_N2 pathway catalyzed by a surface silanol. The inset tables describe which product ketal is formed when R1 and R2 are from the ethanol, C2, or C5 fragments. In S_N2 pathways, Ketals **4b**−**4d** are infeasible due to a tertiary S_N2 reaction or altering the stereochemistry at C5, producing ethyl-sorboside, which was not detected in experiment. All S_N1 pathways invoke the Lewis acid site, which stabilizes the oxygen of the deprotonated hydroxyl on R_2, which transfers its proton to the R_1 hydroxyl either directly (c) or via a surface silanol (d), which stabilizes the deprotonated oxygen. In S_N1 pathways, Ketal **4a** is excluded because it would require forming an unstable primary carbocation and ketal 4d was excluded because stereochemistry changes at C5 would produce ethyl-sorboside, which was not detected in experiment.

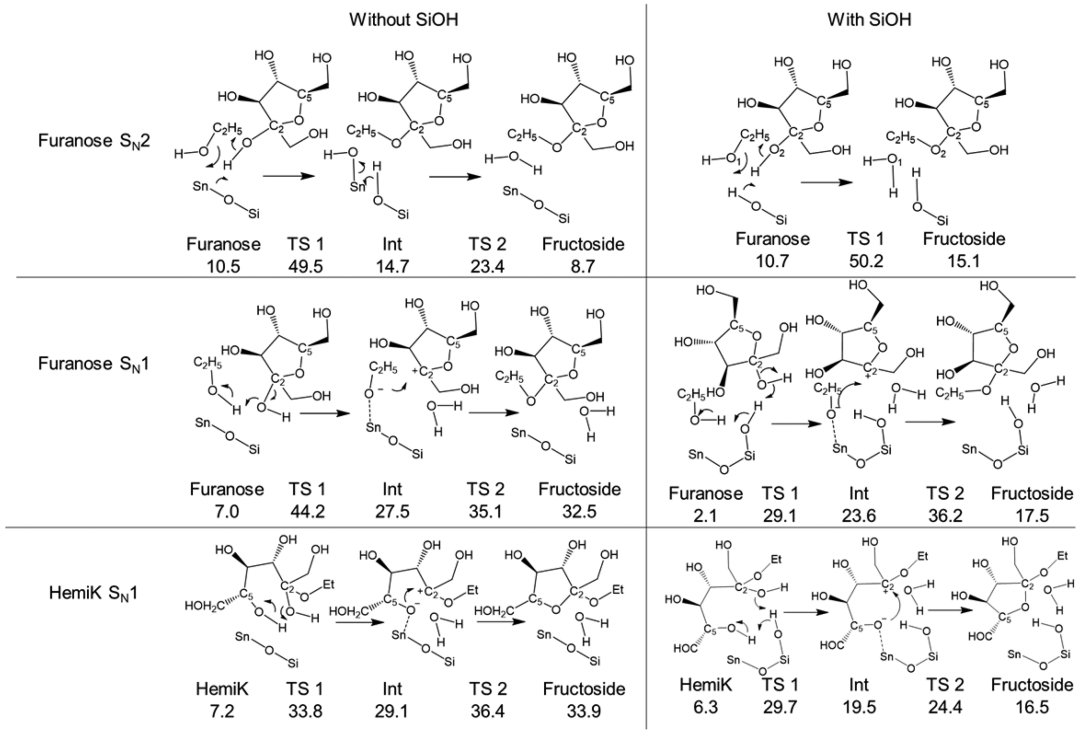

Figure 2. Ketalization reaction pathways. Relative PBE-D3 electronic energies (kcal/mol) are reported with respect to the minimum furanose energy in Figure S2, pathway C. Results computed without dispersion correction are presented in Table S2.

of the alcohol to a Sn−O−Si bridge, forming an SiOH and binding the alcohol O to Sn. The ketone C2 is then attacked by the alkoxy while the SiOH transfers its proton to the ketone O, forming the hemiketal and regenerating the active site. Pathway B starts with the ketone coordinating to the Sn. The alcohol hydroxyl deprotonates to a Sn−O−Si bridge while it attacks the ketone C2, forming a silanol and a deprotonated hemiketal. Protonation of the hemiketal from the silanol produces the hemiketal and regenerates the active site. Pathway C uses a silanol instead of the Sn site and assists a

DOI: 10.1021/acscatal.8b01615
ACS Catal. 2018, 8, 9056−9065

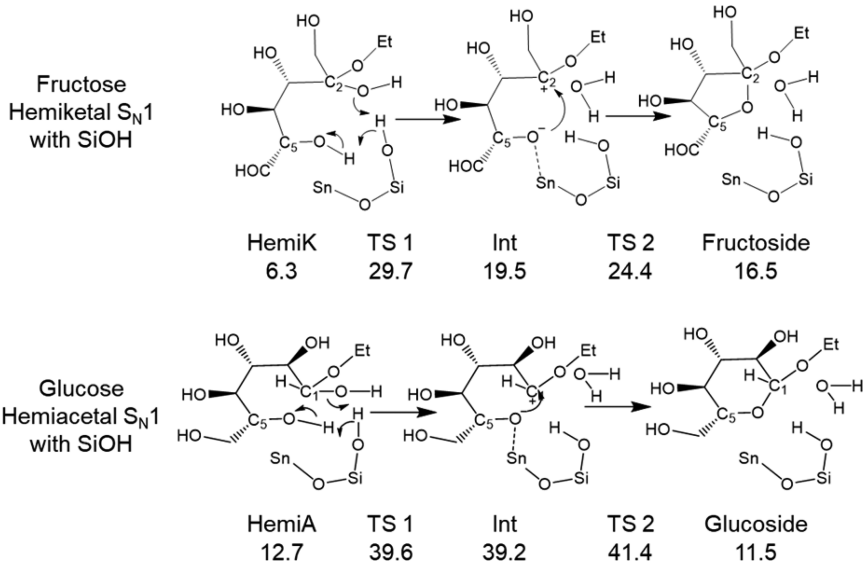

Figure 3. Glucose acetalization compared to fructose ketalization, both following S_N1 mechanisms with SiOH participation. Glucose acetalization is less favorable by over 9 kcal/mol compared to fructose ketalization. Relative PBE-D3 electronic energies (kcal/mol) are reported with respect to the minimum furanose energy in Figure S2, pathway C. Results computed without dispersion correction are presented in Table S3.

proton transfer from the alcohol to the ketone in a concerted step with the C−O bond formation. In all cases, if the alcohol is the O5 hydroxyl, the product is fructofuranose **2**, while if the alcohol is ethanol, the product is hemiketal **3**. Reaction profiles are provided in Figures S1 and S2. Fructose ring-closing is facile, with pathway B giving a low barrier of 14.5 kcal/mol. Hemiketal formation with ethanol favors pathway A and is less favorable than ring-closing, with a barrier of 25.2 kcal/mol.

4.2. Ketalization Mechanisms. Formation of the ketal from either hemiketal involves the C2 hydroxyl reacting with either the ethanol hydroxyl (for fructofuranose **2**) or the O5 hydroxyl (for hemiketal **3**). For each of these intermediates, S_N1 and S_N2 mechanisms are possible, either involving the surface SiOH or not (Scheme 3). This generates a total of 16 distinct potential pathways for consideration (Scheme 3). Primary S_N1 mechanisms can be excluded due to instability of a primary carbocation, so two pathways to **4a** are excluded. This leaves two S_N2 pathways to **4a**, with and without silanol participation (Figure 2). Tertiary S_N2 mechanisms are infeasible due to steric hindrance, so two pathways each to **4b** and **4c** are excluded, leaving two S_N1 pathways each to **4b** and **4c** (Figure 2). Elimination of O5 as H_2O via S_N2 would cause a change in stereochemistry at the C5 of fructose, producing sorbose, and elimination via S_N1 would likely produce a racemic mixture of fructose and sorbose. The Aminex HPX-87C column was used to separate the reaction products[17] and is capable of separating fructose and sorbose; because no sorbose was detected, pathways to ketal **4d** can be ruled out. The six remaining pathways were investigated with DFT; the reaction steps and electronic energy of the intermediates and TS are described in Figure 2.

4.2.1. S_N2 Pathways. In the S_N2 pathway without SiOH participation (Figure 2), the fructose O2 hydroxyl deprotonates to the Sn−O−Si bridge, forming a SiOH, while the fructose O2 attacks ethanol, whose C−OH bond breaks as the ethanol hydroxyl is transferred to the Sn. In a subsequent step, the SnOH and SiOH recombine to regenerate the active site and form the product water. This is similar to the Lewis-acid catalyzed S_N2 etherification mechanism proposed by Christiansen et al.[42] In the S_N2 pathway with SiOH participation, the Sn site is not invoked; instead, a surface silanol shuttles a proton from fructose O2 to ethanol, forming a leaving water molecule as fructose O2 attacks the ethanol CH_2.

Figure 2 shows the reaction mechanisms for the S_N2 pathways. Both the S_N2 pathways computed have very large barriers; 39 kcal/mol without the SiOH participation and 39.5 kcal/mol with the SiOH participation, indicating that this chemistry does not occur via an S_N2 mechanism.

4.2.2. S_N1 Pathways. The S_N1 pathways begin with either ethanol (furanose S_N1) or the fructose O5 hydroxyl (hemiketal S_N1) deprotonating and binding to the Sn site, whose Lewis acidity stabilizes the negative charge, distributing it among the Sn−O−Si bridge oxygens. The proton is transferred to the fructose O2 hydroxyl, either directly (S_N1 without SiOH), or assisted by a surface silanol (S_N1 with SiOH), after which water is removed from C2. This creates a metastable intermediate with the EtO^- (furanose S_N1) or the fructose $O5^-$ (hemiketal S_N1) coordinated to the Sn, as well as the fructose C2 carbocation, which is stabilized by a resonance structure with the oxonium. As such, these pathways bear a resemblance to the S_N1 mechanism for Brønsted-acid catalyzed ketalization,[20] which generates an oxonium after protonation and dehydration of the hemiacetal. The innovation in this Lewis acid case is that the Brønsted proton comes from a substrate alcohol, which is stabilized by the Lewis acid. The final step is to bring the O^- to the R_1 carbocation, forming the final ketal product.

The energetics for the S_N1 pathways are illustrated in Figure 2. Of all these pathways, the HemiK S_N1 with SiOH is most favorable, with a maximum transition state energy at least 6.5 kcal/mol lower than the competing pathways. Of particular note is the importance of the adjacent silanol for stabilizing TS 1, Int, and TS 2, each of these states is 6−8 kcal/mol more stable than the corresponding states in HemiK S_N1 without SiOH, the comparable mechanism without the favorable silanol interaction.

4.3. Glucose Acetalization Pathways. To compare glucose acetalization with fructose ketalization, we carried

DOI: 10.1021/acscatal.8b01615
ACS Catal. 2018, 8, 9056−9065

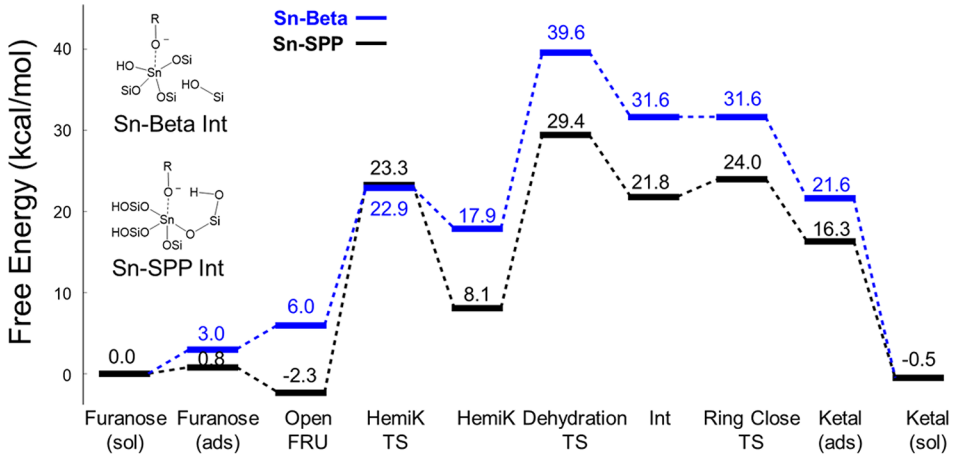

Figure 4. Free energy profiles for fructose ketalization on Sn-SPP and Sn-Beta. Inset scheme highlights key attributes of active site geometry at the key intermediate for ketalization. Sn-Beta has an open site, with a SnOH and an SiOH; however, the SiOH cannot interact favorably with the ketalization intermediates and transition states. Sn-SPP has a closed site with an adjacent surface SiOH group that can interact favorably with the ketalization intermediates and transition states.

out analogous calculations probing the mechanism for a comparable pathway from glucose to ethyl-glucoside, with the same features as the most favorable fructose ketalization pathway. Open glucose reacts with ethanol to form a hemiacetal, followed by an S_N1 acetalization mechanism assisted by the surface SiOH. Although the hemiacetal formed is more stable than the hemiketal, the water removal and ring-closing transition states for acetalization are significantly higher energy than those for ketalization (Figure 3). This is consistent with experiment, in which no ethyl-glucoside is detected.

Although the Lewis acid in Sn-SPP cannot catalyze glucose acetalization, strong Brønsted acids such as sulfonic acid-functionalized SBA-15[43] and H_2SO_4 have been shown to catalyze glucose acetalization, but cause dehydration of fructose and formation of humins instead of fructose ketalization. Weaker Brønsted acids, such as those in H-USY, catalyzed both fructose ketalization and glucose acetalization,[15] but fructose ketalization was 16 times faster than glucose acetalization—indicating a higher barrier for glucose acetalization on this catalyst, as well.

Therefore, we conclude that the selectivity to fructoside is not a unique feature of the Sn-SPP zeolite; rather it is a consequence of an intrinsic difference in reactivity of glucose and fructose. In further support of this, gas-phase calculations (see the Supporting Information and Figure S4) for model hemiacetals and hemiketals show that the proton affinity of the anomeric hydroxyls of hemiketals are 9−12 kcal/mol greater than these of hemiacetals and that oxonium intermediates of hemiketals are 13−14 kcal/mol more stable than those of hemiacetals, both indications of selectivity for ketalization in S_N1 mechanisms.

4.4. Glucose Isomerization. To complete the reaction network, we also computed a reaction pathway from open glucose to open fructose (Figure S3). Following mechanisms for glucose isomerization on Lewis acids,[12,39,41,44−46] we focused on one pathway, in which open glucose binds to the Sn in a bidentate configuration with O1 and O2. In a three-step reaction, O2 deprotonates to the Sn−O−Si bridge, followed by a 1,2-intramolecular H-shift, followed by reprotonation of the O1 hydroxyl. The H-shift is the highest barrier step for this reaction, with a TS energy comparable (30.2 kcal/mol) to the highest point for the ketalization reaction (29.7 kcal/mol), consistent with both products being observed in experiment.

4.5. Comparing Sn-SPP with Sn-Beta. The most favorable ketalization mechanism utilizes a silanol, which donates a proton to the anomeric hydroxyl and also stabilizes the O5 hydroxyl of the hemiketal. In Sn-SPP, this silanol is connected to the Sn site as Sn−O−Si−OH and so is positioned close enough to stabilize the key transition states and intermediates. However, the silanol in the most stable Sn-Beta open site geometries[47] is formed from the hydrolysis of a Sn−O−Si bridge and is not connected to a Sn−O−Si bridge but reaches across the gap created by the hydrolysis. Consequently, only "w/o silanol" mechanisms are feasible; the Sn-Beta silanol cannot assist the ketalization as the Sn−O−Si−OH does in Sn-SPP (Figure 4, inset). The potential energy calculations were used to identify the most favorable reaction pathway for each catalyst, and then harmonic frequencies were calculated for these reaction profiles to estimate relative free energies along the reaction coordinate.

We used Monte Carlo simulations in the Gibbs ensemble to estimate adsorption of fructose onto each Sn site from ethanol solution with ethanol coadsorption (see the Supporting Information). These simulations directly yield the free energy of adsorption via the number densities of fructose in each phase.[48,49] By adding the adsorption free energies to the DFT-calculated free energy profiles, the reaction profiles may be compared with respect to the same liquid-solution reference state. The free energy of transfer for fructose from solution (see Section 5 and the Supporting Information) was calculated to be $\Delta G_{ads} = 0.8 \pm 0.6$ kcal/mol into Sn-SPP and $\Delta G_{ads} = 3 \pm 1.2$ kcal/mol into Sn-Beta. We find that fructose in Sn-SPP is adsorbed only in the mesopore space and excluded from the micropores, as has been observed prior for hexose sugars in MFI.[38] Although not explicitly studied here, the mesoporosity of Sn-SPP likely exhibits enhanced fructose transport relative to Sn-Beta, as well.[50] Adding the fructose adsorption free energies to the DFT-calculated free energy profiles raises the free energy of the first adsorbed furanose intermediate (and all subsequent intermediates) by ΔG_{ads}, giving the profiles presented in Figure 4.

Using the energy span model,[51,52] the relative activation energies and turnover frequencies (TOF) for each catalyst can

DOI: 10.1021/acscatal.8b01615
ACS Catal. 2018, 8, 9056−9065

be estimated, by identifying the TOF-determining intermediate (TDI) and TOF-determining TS (TDTS) for each reaction. In both Sn-Beta and Sn-SPP, the TDTS is the dehydration TS, with free energies of 39.6 and 29.4 kcal/mol, respectively. For Sn-Beta, the TDI is the product ketal in solution, at −0.5 kcal/mol giving an energy span of 40.1 kcal/mol, while for Sn-SPP, the TDI is open fructose, at −2.3, giving an energy span of 31.7 kcal/mol. Consequently, the reaction is dramatically more favorable on Sn-SPP than Sn-Beta. The relatively unfavorable adsorption of fructose into Sn-Beta compounds an already unfavorable reactivity to the ketal.

5. SOLVATION AND ADSORPTION OF FRUCTOSE

The Monte Carlo simulations yield a population of fructose and ethanol molecules in equilibrium between the zeolite and solution phases. At T = 363 K and p = 1.7 bar, ethanol fills both zeolites (for Sn-SPP this includes both the micropores and the mesopores) with a total amount of 638 ± 3 and 209 ± 0.9 molecules in the Sn-SPP system (built from film with 6 MFI unit cells and 67% mesopore volume fraction) and Sn-Beta (18 unit cells), respectively. Fructose competes with ethanol for adsorption in the porous systems, with a total amount of 5 ± 1.6 and 0.6 ± 0.4 in Sn-SPP (including both micropores and mesopores) and Sn-Beta, respectively.

This competitive adsorption of fructose and ethanol into regions near the active site in Sn-SPP can be probed by the density profiles across the micropore and mesopore, as shown in Figure 5. By distinguishing two populations of each adsorbate, those with at least one H-bond to a surface silanol (defined as a fructose or ethanol molecule hydrogen-bonded to an external silanol group by loose criteria[35,53] of $r_{OO} \leq 0.33$ nm and $r_{OH} \leq 0.25$ nm) and those without H-bond to the surface, adsorption to the mesopore surface can be distinguished from adsorption in the "bulk" (for fructose, the "bulk" adsorption is only in the mesopore region, but for ethanol it includes both the micropores and the interior of the mesopore, as seen in Figure 5). Using this definition, 16 ± 12% of adsorbed fructose molecules are hydrogen-bonded to the surface, while about 15.7 ± 0.2% of adsorbed ethanol molecules are hydrogen-bonded to the surface. For ethanol, the density is enriched by a factor of about two on the surface compared to the center of the mesopore. For fructose, however, the density decreases by a factor of about two, demonstrating that fructose must compete with ethanol for adsorption to silanols at the mesopore surface. However, the density of fructose in the center of the mesopore is similar to the density of fructose in solution, corresponding to a nearly negligible free energy of transfer from solution to bulk mesopore.

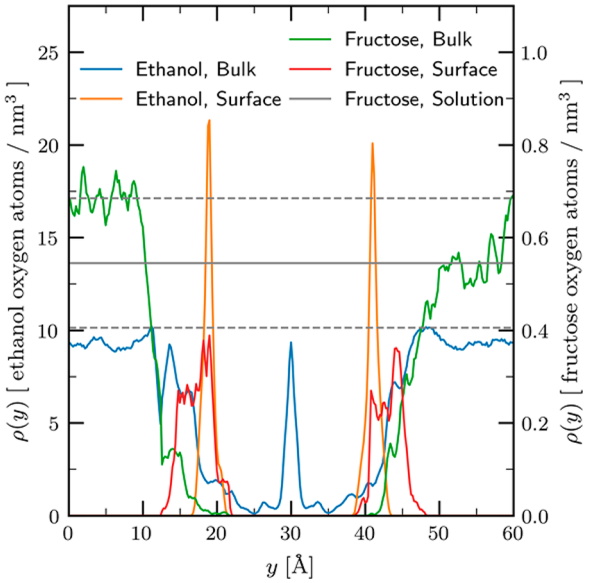

Figure 5. Density profiles (number of oxygen atoms per nm^3) for ethanol (left axis scale) and fructose (right axis scale), as adsorbed in the "bulk" micropore and mesopore interior region (not hydrogen-bonded to silanols) and mesopore "surface" region (hydrogen-bonded to silanols) in SPP. The horizontal lines indicate the density of fructose in the solution phase, along with dashed lines indicating 95% confidence intervals estimated by multiplying the standard error of the mean of eight independent simulations by a factor of 2.4. The micropore (as defined by location of Si atoms on surface silanols) ranges from y = 21.3 to 38.8 Å. The Sn atoms are located at y = 37. Å.

The free energies of transfer are computed using the ratio of number densities between fructose in solution and fructose on the surface of Sn-SPP, as identified by H-bonds with the surface. Consequently, while the free energy of transfer from solution into the entire zeolite box is 0.4 ± 0.4 kcal/mol, the free energy of transfer to the surface of SPP (where the reaction occurs) is 0.8 ± 0.6 kcal/mol, because ethanol enrichment at the surface inhibits the adsorption of fructose. In contrast, the free energy of adsorption into Sn-Beta is 3 ± 1.2 kcal/mol, i.e., adsorption is significantly more unfavorable. More details on these calculations are provided in the Supporting Information.

The differences in solvation of fructose by ethanol in each phase are conveyed in the oxygen (fructose)−oxygen (ethanol) radial distribution functions (RDFs) and number integrals shown in Figure 6a and b, respectively. For Sn-SPP, the RDFs are calculated separately for fructose molecules located either on the "surface" or the "bulk," while the profiles in Sn-Beta or solution are independent of location.

Because fructose only adsorbs in the mesopores (see Figure 5), the solvation of fructose in the "bulk" of Sn-SPP by ethanol is similar to its solvation in solution. The shape of the RDFs in solution and in the Sn-SPP bulk are very similar, indicating similar coordination of ethanol around fructose. The RDF in Sn-SPP is shifted upward relative to that in solution. This is because the majority of pairwise distances occur at short distances in the mesopore, while the RDF is normalized by the entire box volume which includes a smaller number of longer-distance pairs between fructose in the mesopore and ethanol in the micropore. Nonetheless, the number integrals for the two up to approximately 5 angstrom are quite similar in number and shape, with a slightly smaller coordination number in the Sn-SPP bulk than in the Sn-SPP solution, and a slightly smaller coordination number in the higher-concentrated Sn-BEA solution. These observations are in line with a nearly negligible free energy of transfer for fructose from solution to the bulk mesopore of Sn-SPP.

For adsorbates H-bonded to surface silanols, the RDF from fructose to ethanol indicates only one clear solvation shell. Interestingly, the corresponding number integral (surface fructose to surface ethanol) is similar in magnitude to that for molecules adsorbed in Sn-Beta, indicating that fructose molecules in both regions are surrounded by a similar number of ethanol molecules. The RDF from fructose on the surface of Sn-SPP to bulk ethanol in the mesopores and micropores has slightly more ordered coordination than that to surface

DOI: 10.1021/acscatal.8b01615
ACS Catal. 2018, 8, 9056−9065

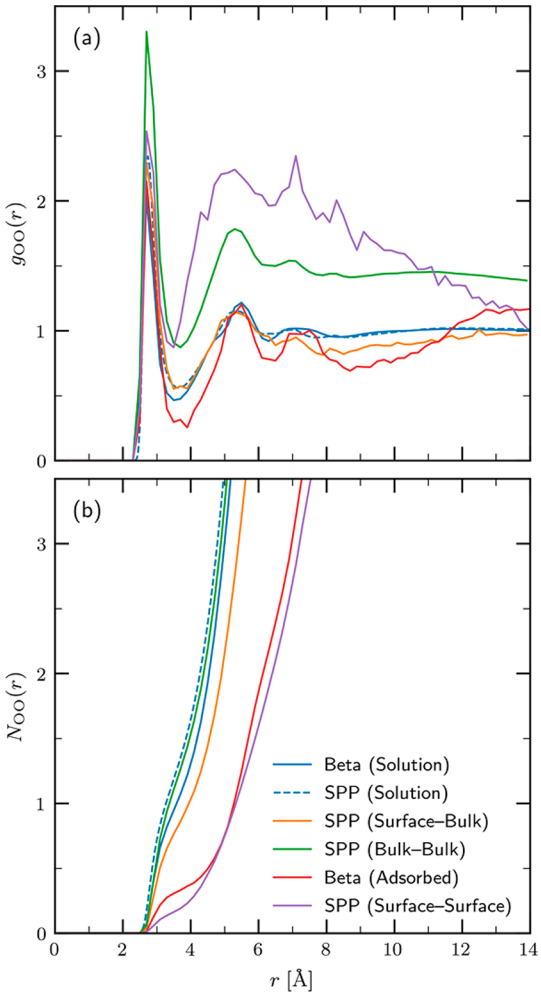

Figure 6. Fructose oxygen−ethanol oxygen (a) radial distribution functions and (b) number integrals in the solution phase, Sn-Beta, and in different regions of Sn-SPP as determined from the molecular simulations. "Surface" refers to fructose or ethanol molecules hydrogen-bonded to a surface silanol, and "Bulk" refers to those molecules not hydrogen-bonded to a surface silanol.

ethanol, while the RDF in Sn-BEA has the clearest coordination shells of those in a zeolite phase. The number of ethanol molecules in the bulk surrounding fructose adsorbed to the surface of Sn-SPP is much higher than those surrounding fructose in Sn-BEA, due to the high density of ethanol in the mesopores of Sn-SPP. A more favorable ethanolic solvation of fructose adsorbed onto the active site of Sn-SPP than Sn-BEA is attributed to lead to the former's more favorable free energy of adsorption.

6. CONCLUSIONS

The Sn-SPP zeolite is capable of catalyzing the selective ketalization of fructose in the presence of glucose specifically due to the activity of its Sn−O−Si−OH moiety. The silanol shuttles the proton from the O5 hydroxyl to the O2 hydroxyl to remove it as water and also stabilizes the deprotonated O5 hydroxyl along with the Lewis acidic Sn. The Sn-Beta open site cannot catalyze ketalization because its silanol is too distant from the Sn site to stabilize the deprotonated O5 hydroxyl. Glucose acetalization is not catalyzed by Sn-SPP because the oxonium ion intermediate for glucose acetalization is much less stable than that of fructose. Strong Brønsted acids are too harsh for catalyzing fructose and have been shown to activate acetalization of glucose and dehydration of fructose to side products. In contrast, the surface silanols of Sn-SPP, positioned to work in concert with the Lewis acidic Sn site, form a gentler catalyst that selectively ketalizes fructose without dehydrating it. This catalytic effect is further enhanced through a less unfavorable free energy of adsorption for fructose from solution into Sn-SPP relative to Sn-Beta.

■ ASSOCIATED CONTENT

Supporting Information

Additional reaction profiles on Sn-SPP, an examination of the role of dispersion corrections on the reaction pathways, a table with free energy contributions to the reaction pathway, a comparison of stabilities of model oxonium intermediates in the gas phase, and additional detailed methods and results for Gibbs ensemble Monte Carlo simulations. The Supporting Information is available free of charge on the ACS Publications website at DOI: 10.1021/acscatal.8b01615.

Additional reaction profiles on Sn-SPP, an examination of the role of dispersion corrections on the reaction pathways, a table with free energy contributions to the reaction pathway, a comparison of stabilities of model oxonium intermediates in the gas phase, and additional detailed methods and results for Gibbs ensemble Monte Carlo simulations (PDF)

Additional molceular structures (ZIP)

■ AUTHOR INFORMATION

Corresponding Author

*E-mail: josep180@umn.edu.

ORCID

Tyler R. Josephson: 0000-0002-0100-0227
Michael Tsapatsis: 0000-0001-5610-3525
J. Ilja Siepmann: 0000-0003-2534-4507
Dionisios G. Vlachos: 0000-0002-6795-8403
Stavros Caratzoulas: 0000-0001-9599-4199

Notes

The authors declare no competing financial interest.

■ ACKNOWLEDGMENTS

Financial support through the Catalysis Center for Energy Innovation, a U.S. Department of Energy − Energy Frontier Research Center under Grant No. DE-SC0001004, is gratefully acknowledged. Computational resources were provided by the National Energy Research Scientific Computing Center (NERSC), which is supported by the Office of Science of the U.S. Department of Energy under Contract DE-AC02-05CH11231, Information Technologies (IT) at the University of Delaware, and the Minnesota Supercomputing Institute (MSI) at the University of Minnesota.

■ REFERENCES

(1) Kamm, B.; Gruber, P. R.; Kammm, M. *Biorefineries − Industrial Processes and Products*; Wiley-VCH: Weinheim, Germany, 2010.

(2) Jong, E. d.; Higson, A.; Walsh, P.; Wellisch, M. Biobased Chemicals - Value Added Products from Biorefineries. *IEA Bioenergy-Task* **2011**, *42*, 36.

(3) Ragauskas, A. J.; Williams, C. K.; Davison, B. H.; Britovsek, G.; Cairney, J.; Eckert, C. A.; Frederick, W. J., Jr.; Hallett, J. P.; Leak, D. J.; Liotta, C. L.; Mielenz, J. R.; Murphy, R.; Templer, R.; Tschaplinski,

DOI: 10.1021/acscatal.8b01615
ACS Catal. 2018, 8, 9056−9065

T. The Path Forward for Biofuels and Biomaterials. *Science* **2006**, *311*, 484−489.
(4) Huber, G. W. Breaking the Chemical and Engineering Barriers to Lignocellulosic Biofuels : Next Generation Hydrocarbon Biorefineries. *NSF* **2008**, *1*−*177*. DOI: 10.2172/1218335
(5) Huber, G. W.; Corma, A. Synergies between Bio- and Oil Refineries for the Production of Fuels from Biomass. *Angew. Chem., Int. Ed.* **2007**, *46*, 7184−7201.
(6) Tong, X.; Ma, Y.; Li, Y. Biomass into Chemicals: Conversion of Sugars to Furan Derivatives by Catalytic Processes. *Appl. Catal., A* **2010**, *385*, 1−13.
(7) Rosatella, A. A.; Simeonov, S. P.; Frade, R. F. M.; Afonso, C. A. M. 5-Hydroxymethylfurfural (HMF) as a Building Block Platform: Biological Properties, Synthesis and Synthetic Applications. *Green Chem.* **2011**, *13*, 754.
(8) Van Putten, R. J.; Van Der Waal, J. C.; De Jong, E.; Rasrendra, C. B.; Heeres, H. J.; De Vries, J. G. Hydroxymethylfurfural, a Versatile Platform Chemical Made from Renewable Resources. *Chem. Rev.* **2013**, *113*, 1499−1597.
(9) Van Putten, R. J.; Soetedjo, J. N.; Pidko, E. A.; van der Waal, J. C.; Hensen, E. J.; de Jong, E.; Heeres, H. J. Dehydration of Different Ketoses and Aldoses to 5-Hydroxymethylfurfural. *ChemSusChem* **2013**, *6*, 1681−1687.
(10) Moliner, M.; Román-Leshkov, Y.; Davis, M. E. Tin-Containing Zeolites Are Highly Active Catalysts for the Isomerization of Glucose in Water. *Proc. Natl. Acad. Sci. U. S. A.* **2010**, *107*, 6164−6168.
(11) Choudhary, V.; Pinar, A. B.; Sandler, S. I.; Vlachos, D. G.; Lobo, R. F. Xylose Isomerization to Xylulose and Its Dehydration to Furfural in Aqueous Media. *ACS Catal.* **2011**, *1*, 1724−1728.
(12) Bermejo-Deval, R.; Assary, R. S. S.; Nikolla, E.; Moliner, M.; Roman-Leshkov, Y.; Hwang, S.-J. S.-J.; Palsdottir, A.; Silverman, D.; Lobo, R. F.; Curtiss, L. A.; Davis, M. E. Metalloenzyme-like Catalyzed Isomerizations of Sugars by Lewis Acid Zeolites. *Proc. Natl. Acad. Sci. U. S. A.* **2012**, *109*, 9727−9732.
(13) Takasaki, Y. Studies on Sugar-Isomerizing Enzyme. *Agric. Biol. Chem.* **1966**, *30*, 1247−1253.
(14) Saravanamurugan, S.; Paniagua, M.; Melero, J. A.; Riisager, A. Efficient Isomerization of Glucose to Fructose over Zeolites in Consecutive Reactions in Alcohol and Aqueous Media. *J. Am. Chem. Soc.* **2013**, *135*, 5246−5249.
(15) Saravanamurugan, S.; Riisager, A.; Taarning, E.; Meier, S. Combined Function of Brønsted and Lewis Acidity in the Zeolite-Catalyzed Isomerization of Glucose to Fructose in Alcohols. *ChemCatChem* **2016**, *8*, 3107−3111.
(16) Rubio-Caballero, J. M.; Saravanamurugan, S.; Maireles-Torres, P.; Riisager, A. Acetalization of Furfural with Zeolites under Benign Reaction Conditions. *Catal. Today* **2014**, *234*, 233−236.
(17) Ren, L.; Guo, Q.; Kumar, P.; Orazov, M.; Xu, D.; Alhassan, S. M.; Mkhoyan, K. A.; Davis, M. E.; Tsapatsis, M. Self-Pillared, Single-Unit-Cell Sn-MFI Zeolite Nanosheets and Their Use for Glucose and Lactose Isomerization. *Angew. Chem., Int. Ed.* **2015**, *54*, 10848−10851.
(18) Ren, L.; Guo, Q.; Orazov, M.; Xu, D.; Politi, D.; Kumar, P.; Alhassan, S. M.; Mkhoyan, K. A.; Sidiras, D.; Davis, M. E.; Tsapatsis, M. Pillared Sn-MWW Prepared by a Solid-State-Exchange Method and Its Use as a Lewis Acid Catalyst. *ChemCatChem* **2016**, *8*, 1274−1278.
(19) Cho, H. J.; Dornath, P.; Fan, W. Synthesis of Hierarchical Sn-MFi as Lewis Acid Catalysts for Isomerization of Cellulosic Sugars. *ACS Catal.* **2014**, *4*, 2029−2037.
(20) Clayden, J.; Greeves, N.; Warren, S.; Wothers, P. *Organic Chemistry*; 2001.
(21) Mortensen, J.; Hansen, L.; Jacobsen, K. Real-Space Grid Implementation of the Projector Augmented Wave Method. *Phys. Rev. B: Condens. Matter Mater. Phys.* **2005**, *71*, 035109.
(22) Enkovaara, J.; Rostgaard, C.; Mortensen, J. J.; Chen, J.; Dułak, M.; Ferrighi, L.; Gavnholt, J.; Glinsvad, C.; Haikola, V.; Hansen, H. A.; Kristoffersen, H. H.; Kuisma, M.; Larsen, A. H.; Lehtovaara, L.; Ljungberg, M.; Lopez-Acevedo, O.; Moses, P. G.; Ojanen, J.; Olsen, T.; Petzold, V.; Romero, N. A.; Stausholm-Møller, J.; Strange, M.; Tritsaris, G. A.; Vanin, M.; Walter, M.; Hammer, B.; Häkkinen, H.; Madsen, G. K. H.; Nieminen, R. M.; Nørskov, J. K.; Puska, M.; Rantala, T. T.; Schiøtz, J.; Thygesen, K. S.; Jacobsen, K. W. Electronic Structure Calculations with GPAW: A Real-Space Implementation of the Projector Augmented-Wave Method. *J. Phys.: Condens. Matter* **2010**, *22*, 253202.
(23) Bahn, S. R.; Jacobsen, K. W. An Object-Oriented Scripting Interface to a Legacy Electronic Structure Code. *Comput. Sci. Eng.* **2002**, *4*, 56−66.
(24) Blöchl, P. E. Projector Augmented-Wave Method. *Phys. Rev. B: Condens. Matter Mater. Phys.* **1994**, *50*, 17953−17979.
(25) Kresse, G. From Ultrasoft Pseudopotentials to the Projector Augmented-Wave Method. *Phys. Rev. B: Condens. Matter Mater. Phys.* **1999**, *59*, 1758−1775.
(26) Perdew, J. P.; Burke, K.; Ernzerhof, M. Generalized Gradient Approximation Made Simple. *Phys. Rev. Lett.* **1996**, *77*, 3865−3868.
(27) Liu, D. C.; Nocedal, J. On the Limited Memory Method for Large Scale Optimization. *Math. Program. B* **1989**, *45*, 503−528.
(28) Henkelman, G.; Uberuaga, B. P.; Jónsson, H. Climbing Image Nudged Elastic Band Method for Finding Saddle Points and Minimum Energy Paths. *J. Chem. Phys.* **2000**, *113*, 9901−9904.
(29) Henkelman, G.; Jónsson, H. A Dimer Method for Finding Saddle Points on High Dimensional Potential Surfaces Using Only First Derivatives. *J. Chem. Phys.* **1999**, *111*, 7010−7022.
(30) Olsen, R. A.; Kroes, G. J.; Henkelman, G.; Arnaldsson, A.; Jónsson, H. Comparison of Methods for Finding Saddle Points without Knowledge of the Final States. *J. Chem. Phys.* **2004**, *121*, 9776−9792.
(31) Heyden, A.; Bell, A. T.; Keil, F. J. Efficient Methods for Finding Transition States in Chemical Reactions: Comparison of Improved Dimer Method and Partitioned Rational Function Optimization Method. *J. Chem. Phys.* **2005**, *123*, 224101.
(32) Kästner, J.; Sherwood, P. Superlinearly Converging Dimer Method for Transition State Search. *J. Chem. Phys.* **2008**, *128*, 014106.
(33) Larsen, A. H.; Vanin, M.; Mortensen, J. J.; Thygesen, K. S.; Jacobsen, K. W. Localized Atomic Basis Set in the Projector Augmented Wave Method. *Phys. Rev. B: Condens. Matter Mater. Phys.* **2009**, *80*, 1−10.
(34) Grimme, S.; Antony, J.; Ehrlich, S.; Krieg, H. A Consistent and Accurate Ab Initio Parametrization of Density Functional Dispersion Correction (DFT-D) for the 94 Elements H-Pu. *J. Chem. Phys.* **2010**, *132*, 154104.
(35) Bai, P.; Siepmann, J. I.; Deem, M. W. Adsorption of Glucose into Zeolite Beta from Aqueous Solution. *AIChE J.* **2013**, *59*, 3523−3529.
(36) DeJaco, R. F.; Elyassi, B.; Dorneles de Mello, M.; Mittal, N.; Tsapatsis, M.; Siepmann, J. I. Understanding the Unique Sorption of Alkane- α, ω -Diols in Silicalite-1. *J. Chem. Phys.* **2018**, *149*, 072331.
(37) Zhang, X.; Liu, D.; Xu, D.; Asahina, S.; Cychosz, K. A.; Agrawal, K. V.; Al Wahedi, Y.; Bhan, A.; Al Hashimi, S.; Terasaki, O.; Thommes, M.; Tsapatsis, M. Synthesis of Self-Pillared Zeolite Nanosheets by Repetitive Branching. *Science* **2012**, *336*, 1684−1687.
(38) Orazov, M.; Davis, M. E. Tandem Catalysis for the Production of Alkyl Lactates from Ketohexoses at Moderate Temperatures. *Proc. Natl. Acad. Sci. U. S. A.* **2015**, *112*, 201516466.
(39) Yang, G.; Pidko, E. A.; Hensen, E. J. M. The Mechanism of Glucose Isomerization to Fructose over Sn-BEA Zeolite: A Periodic Density Functional Theory Study. *ChemSusChem* **2013**, *6*, 1688−1696.
(40) Li, Y. P. P.; Head-Gordon, M.; Bell, A. T. T. Analysis of the Reaction Mechanism and Catalytic Activity of Metal-Substituted Beta Zeolite for the Isomerization of Glucose to Fructose. *ACS Catal.* **2014**, *4*, 1537−1545.
(41) Brand, S. K.; Josephson, T. R.; Labinger, J. A.; Caratzoulas, S.; Vlachos, D. G.; Davis, M. E. Methyl-Ligated Tin Silsesquioxane Catalyzed Reactions of Glucose. *J. Catal.* **2016**, *341*, 62−71.
(42) Christiansen, M. A.; Mpourmpakis, G.; Vlachos, D. G. Density Functional Theory-Computed Mechanisms of Ethylene and Diethyl

DOI: 10.1021/acscatal.8b01615
ACS Catal. 2018, 8, 9056−9065

Ether Formation from Ethanol on γ-Al2O3(100). *ACS Catal.* **2013**, *3*, 1965−1975.
(43) Saravanamurugan, S.; Riisager, A. Solid Acid Catalysed Formation of Ethyl Levulinate and Ethyl Glucopyranoside from Mono- and Disaccharides. *Catal. Commun.* **2012**, *17*, 71−75.
(44) Rai, N.; Caratzoulas, S.; Vlachos, D. G. Role of Silanol Group in Sn-Beta Zeolite for Glucose Isomerization and Epimerization Reactions. *ACS Catal.* **2013**, *3*, 2294−2298.
(45) Christianson, J. R.; Caratzoulas, S.; Vlachos, D. G. Computational Insight into the Effect of Sn-Beta Na Exchange and Solvent on Glucose Isomerization and Epimerization. *ACS Catal.* **2015**, *5*, 5256−5263.
(46) Li, S.; Josephson, T.; Vlachos, D. G.; Caratzoulas, S. The Origin of Selectivity in the Conversion of Glucose to Fructose and Mannose in Sn-BEA and Na-Exchanged Sn-BEA Zeolites. *J. Catal.* **2017**, *355*, 11.
(47) Josephson, T. R.; Jenness, G. R.; Vlachos, D. G.; Caratzoulas, S. Distribution of Open Sites in Sn-Beta Zeolite. *Microporous Mesoporous Mater.* **2017**, *245*, 45−50.
(48) Martin, M. G.; Siepmann, J. I. Calculating Gibbs Free Energies of Transfer from Gibbs Ensemble Monte Carlo Simulations. *Theor. Chem. Acc.* **1998**, *99*, 347−350.
(49) Ben-Naim, A. *Statistical Thermodynamics for Chemists and Biochemists*; Plenum Press: New York, 1992.
(50) Bai, P.; Haldoupis, E.; Dauenhauer, P. J.; Tsapatsis, M.; Siepmann, J. I. Understanding Diffusion in Hierarchical Zeolites with House-of-Cards Nanosheets. *ACS Nano* **2016**, *10*, 7612−7618.
(51) Kozuch, S.; Shaik, S. How to Conceptualize Catalytic Cycles? The Energetic Span Model. *Acc. Chem. Res.* **2011**, *44*, 101−110.
(52) Kozuch, S. Steady State Kinetics of Any Catalytic Network: Graph Theory, the Energy Span Model, the Analogy between Catalysis and Electrical Circuits, and the Meaning of "Mechanism. *ACS Catal.* **2015**, *5*, 5242−5255.
(53) Dejaco, R. F.; Bai, P.; Tsapatsis, M.; Siepmann, J. I. Adsorptive Separation of 1-Butanol from Aqueous Solutions Using MFI-and FER-Type Zeolite Frameworks: A Monte Carlo Study. *Langmuir* **2016**, *32*, 2093−2101.

DOI: 10.1021/acscatal.8b01615
ACS Catal. 2018, 8, 9056−9065